Bioactive Titanium Surfaces Enriched with Silver Nanoparticles Through an In Situ Reduction: Looking for a Balance Between Cytocompatibility and Antibacterial Activity

Terms of use:

Publisher copyright

(Article begins on next page)

20 April 2024

Bioactive Titanium Surfaces Enriched with Silver Nanoparticles Through an In Situ Reduction: Looking for a Balance Between Cytocompatibility and Antibacterial Activity

Martina Cazzola, Jacopo Barberi,* Sara Ferraris, Andrea Cochis, Grzegorz Cempura, Aleksandra Czyrska-Filemonowicz, Lia Rimondini, and Silvia Spriano*

This research aims toward an antibacterial and osteoconductive Ti_6Al_4V surface by chemical etching–oxidation treatment and in situ reduction of silver nanoparticles. Starting from a previously developed process, already proved to enhance the osteoinductive ability of titanium, different parameters are changed to tailor the amount of silver and its distribution across the surface oxide layer thickness. The samples are characterized by scanning and transmission electron microscopy, energy-dispersive X-ray spectroscopy, release of silver, biofilm formation (*Staphylococcus aureus*), and cytocompatibility toward human osteoblasts progenitor cells. The total amount of silver in the surface oxide layer depends only on the concentration of the silver precursor. The time of the addition of the silver precursor, during the oxidation treatment, affects the oxide layer thickness, dimension, and distribution of the nanoparticles across the surface oxide: they are larger and accumulate on the outermost layer, if the addition occurs early. The maximum ion release occurs after 24 h and lasts up to 14 days; the later addition of silver precursors leads to sustaining the silver release for a longer time. The samples prepared with the higher concentration of the silver precursor are bactericide, but highly cytotoxic, whereas the other ones are bacteriostatic and moderately cytotoxic.

1. Introduction

The peri-implant infections are usually treated with systemic administration and/or local use during the surgery of antibiotics, but these strategies are not able to act against biofilm formation and can induce resistance of the bacterial strains.[1] A chronic infection can lead to the removal and replacement of the prosthesis with high stress and pain for the patients and increasing hospitalization time and costs. The addition of passive (antimicrofouling) and active antibacterial properties to the implant surface can effectively prevent the biofilm formation, thus, reducing the risk of peri-implant infection. Silver nanoparticles can be effective at this purpose. They have different possible mechanisms of action against bacteria: release of silver ions with actions against adenosine triphosphate (ATP) production and DNA replication, generation of reactive oxygen species (ROS), and direct damage of bacteria membrane by the formation of irreversible pores affecting the homeostasis.[2] Silver is not selective and it binds every chemical or biological compound which it is affine to (amines, thiols, phosphates, and silenols). For this reason, it is difficult to identify a specific receptor or binding site activating the pathway for its biological activity; nevertheless, it is due to the lack of selectivity that the broad-spectrum activity of silver as well as the difficulty of bacteria in developing resistance mechanisms can be explained.

The challenging key points are to exploit an antibacterial activity as long as possible (to prevent infections till the complete sealing of the implant to the naïve tissue) and to find a balance between the cytocompatibility and antibacterial activity of silver when it is added to a titanium surface. Several data are available concerning the cytocompatibility and the minimum inhibitory concentration (MIC) of colloidal silver nanoparticles, but further research is needed to clarify the effects of silver when embedded into a surface in contact with cells and bacteria. MIC between 3 and $180\,mg\,l^{-1}$ was reported to be effective toward several bacterial strains including *Escherichia coli*, *Staphylococcus aureus*, and *Staphylococcus epidermis* for silver ions and nanoparticles

M. Cazzola, J. Barberi, S. Ferraris, S. Spriano
DISAT Department
Politecnico di Torino
Corso Duca degli Abruzzi 24, 10129 Torino, Italy
E-mail: jacopo.barberi@polito.it; silvia.spriano@polito.it

A. Cochis, L. Rimondini
Department of Health Sciences, Medical School
Università del Piemonte Orientale
Corso Trieste 15/A, 28100 Novara, Italy

G. Cempura, A. Czyrska-Filemonowicz
AGH University of Science and Technology
al. A. Mickiewicza 30, 30-059 Kraków, Poland

The ORCID identification number(s) for the author(s) of this article can be found under https://doi.org/10.1002/adem.202200883.

**ADVANCED
SCIENCE NEWS**

www.advancedsciencenews.com

**ADVANCED
ENGINEERING
MATERIALS**

www.aem-journal.com

with diameter between 3 and 95 nm.[3–5] The threshold for cytotoxicity of silver nanoparticles is around $60\,mg\,L^{-1}$ for human fibroblasts, whereas cytotoxicity of silver ions has been detected already in solutions with concentration of few $mg\,L^{-1}$.[4,5] A range between 10 and $50\,mg\,L^{-1}$ of silver nanoparticles in suspensions seems to be a good compromise to get an antibacterial activity without cytotoxic effects, but it must be considered that the antibacterial activity of silver nanoparticles depends on several parameters such as size, shape, surface chemistry, and surface charge. Size-dependent effects of silver nanoparticles have been highlighted in many articles that come to the same conclusion: the size of nanoparticles in a suspension should be under 50 nm for being effective against bacteria and nanoparticles around 10–15 nm have increased stability and activity.[2,6–8] This conclusion can be used as a basis to investigate the biological activity of silver nanoparticles embedded into a titanium surface.

It was already shown that the addition of gallic acid (GA) and polyvinyl alcohol (PVA), when a silver precursor is added during the oxidation process of the titanium alloy, is effective to get a much more controlled and uniform distribution of silver nanoparticles on the surface.[9] The chemical reducing activity of polyphenols can be exploited to obtain a higher amount of nanoparticles, using the GA as an additive, whereas the PVA stabilizes the formed nanoparticles avoiding the formation of aggregates.

The authors have already investigated chemically treated titanium surfaces for bone implants both with[9,10] and without[11–13] the addition of silver during the chemical treatment (oxidation process). The treated surfaces are bioactive, meaning that they lead to the precipitation of hydroxyapatite in contact with the physiological fluids, improving the biological response, and discouraging bacteria adhesion.[14,15] An active antibacterial action can be achieved when silver is incorporated into the surface oxide layer.[9,10]

The aim of this research is to explore the effect of changing the concentration of the silver precursor and time when it is added during the oxidation process. This is expected to change the amount and the distribution of silver across the thickness of the oxide layer and, as a consequence, the amount and duration of the silver release, as well as the surface density of nanoparticles exposed to a direct contact with bacteria and/or cells. Accordingly, in this work such new surfaces have been characterized and compared both from the chemical–physical and biological standpoints.

2. Results and Discussion

In this research, an optimization of the synthesis of silver-doped Ti_6Al_4V surfaces is performed based on previous works.[9,10]

A focus on the best time of addition of the silver precursor and additives during the chemical process is made here. Three types of samples prepared by adding the silver precursor and additives at different times of the oxidation process are prepared and compared to investigate the effect of an early (CT_Ad + Ag (0.005 M)_T1), intermediate (CT_Ad + Ag (0.005 M)_T2), or late (CT_Ad + Ag(0.005 M)_T3) addition. A fourth type of sample is prepared by following the protocol T2 but changing the concentration of the silver precursor during the process (CT_Ad + Ag(0.001 M)_T2). A reference type of sample without the silver addition (CT) is used as reference, when needed.

2.1. Surface Characterization

The surface of all the samples was investigated by field-emission scanning electron microscopy (FESEM) observation and energy-dispersive X-ray spectroscopy (EDS) analysis. The micrographs of CT, CT_Ad + Ag (0.005 M)_T1, CT_Ad + Ag (0.005 M)_T2, and CT_Ad + Ag(0.001 M)_T2 are reported in **Figure 1**, whereas the EDS results of all the samples are reported in **Table 1**.

The morphology of the chemically treated surface (CT) is nanoporous as already described,[11] and it is analogous on all the samples with or without silver. The presence of the silver nanoparticles is barely visible on the sample CT_Ad + Ag(0.005 M)_T1 where nanoparticles of few tens of nanometers in diameter decorate the ridges of the nanopores, whereas it is not possible to see the nanoparticles by FESEM on all the other samples. The appearance of CT_Ad + Ag (0.005 M)_T3 is analogous to CT_Ad + Ag (0.005 M)_T2 and it was not reported.

The presence of silver nanoparticles with diameter lower than 10 nm or of silver ions dispersed in the titanium oxide sponge-like structure can be hypothesized at this stage on the surfaces where the nanoparticles are not observable (CT_Ad + Ag (0.005 M)_T2, CT_Ad + Ag (0.005 M)_T3, and CT_Ad + Ag (0.001 M)_T2). Looking at the EDS results, the presence of a high amount of oxygen on all the samples agrees with the formation of a surface oxide layer during the chemical treatment. Vanadium is detected in a low amount on all the surfaces. It can be assumed that the penetration depth of the EDS analysis is larger than the thickness of the surface oxide layer, in fact the thickness of the oxide layer has been estimated as 400 nm[13] and the penetration depth of EDS analyses is around 1 μm. Moreover, since the surface oxide is not expected to contain vanadium,[16] the signal of vanadium comes from the metal alloy that is below the surface
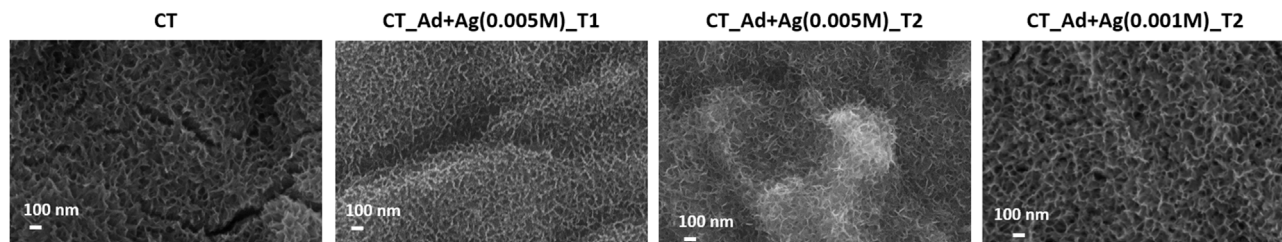

Figure 1. FESEM micrographs of the samples CT, CT_Ad + Ag (0.005 M)_T1, CT_Ad + Ag (0.005 M)_T2, and CT_Ad + Ag (0.00 1 M)_T2 at the magnification of 150.00 k×.

**ADVANCED
SCIENCE NEWS**

www.advancedsciencenews.com

**ADVANCED
ENGINEERING
MATERIALS**

www.aem-journal.com

Table 1. EDS analysis of the treated samples.

Elements [at%]	CT	CT_Ad + Ag (0.005 M)_T1	CT_Ad + Ag (0.005 M)_T2	CT_Ad + Ag (0.005 M)_T3	CT_Ad + Ag (0.00 1 M)_T2
O	53.91	44.29	53.39	53.38	48.72
Al	4.44	5.39	4.74	3.94	4.93
Ti	40.13	47.98	39.87	40.67	44.83
Ag	–	0.75	0.86	0.92	0.33
V	1.52	1.59	1.13	1.10	1.20

oxide layer. On this basis, the reported EDS analysis refers to the average chemical composition of all the surface oxide layer throughout its thickness, with a small contribution of the underlying metal alloy. Silver has been detected by EDS on all the analyzed surfaces. Looking at the EDS results of the samples prepared with 0.005M AgNO$_3$, a similar silver content is detected on all the samples. As expected, the silver amount is lower on CT_Ad + Ag (0.001 M)_T2 because of the larger dilution of the silver precursor.

The X-ray photoelectron spectroscopy (XPS) analysis was performed to better investigate the chemical composition of the outermost layer (5–10 nm) of the treated samples and the chemical oxidation state of the silver embedded into the oxide layer. The analysis has been performed on three specimens nominally identical. The results are reported in **Table 2** as mean and standard deviation of the atomic percentages. The XPS chemical analysis of CT is reported as reference.

The main detected elements are oxygen, carbon, titanium, silver, and small percentages of other elements as contaminants. Oxygen and titanium are detected on all the samples because of the presence of the titanium oxide layer. Their content is lower on the samples treated with the silver addition (CT_Ad + Ag (0.00 5 M)_T1, CT_Ad + Ag (0.005 M)_T2, and CT_Ad + Ag (0.005 M)_T3) with respect to CT because they are partially substituted by silver. The content of carbon is partially due to the unavoidable surface contamination of titanium surfaces,[17] but it is higher on the samples treated with the addition of the additives and silver; and it could be correlated to the presence of residues of PVA and GA. Looking at the Ag atomic concentration obtained by the XPS analyses, there is a lower content of silver on the outermost layer of CT_Ad + Ag (0.005 M)_T2 with respect to CT_Ad + Ag(0.005 M)_T1. A great standard deviation of the values detected on CT_Ad + Ag (0.005 M)_T3 does not allow a comparison of this surface with the others; a nonuniform distribution of silver occurs on this surface. As expected, the amount of Ag detected on CT_Ad + Ag (0.001 M)_T2 is the

lowest of all, which is consistent with the EDS results reported in Table 1.

The profile fitting of the high-resolution spectra of the oxygen and silver regions was performed to investigate the oxidation state of these elements.

In **Figure 2**, the same peaks are visible in the oxygen region of the spectra of all the samples. The same four contributions have been found on all samples, namely, from Ti–O ($\approx$529.8/530.0 eV), −OH groups, which can be split into acidic −OH (−OH$_a$)($\approx$530.7 eV) and basic −OH (−OH$_b$)($\approx$530.7 ev), and, at last, from adsorbed water ($\approx$532.7 eV).[18–20] Those results are consistent with a work previously published by the authors.[13] A contribution to the −OH signal due to residues of GA cannot be completely excluded in the case of the samples treated with the addition of the silver precursor and additives.[21] The presence of a high density of −OH groups on CT is of interest because it can be hypothesized that they have a role in the in situ reduction of silver, when the silver precursor is added during the sample preparation. It has been reported in the literature that hydroxyls can reduce silver ions in some conditions,[22] and −OH groups can act as nucleation points for AgNPs by complexing Ag$^+$ ions.[23] On CT samples, dissociated −OH$_a$ groups may have a double effect toward the formation of silver nanoparticles; they can directly reduce silver from ionic to metallic, or they can increase the concentration of Ag$^+$ near the surface of titanium enhancing nucleation and clustering of silver atoms, once they have been reduced by GA. A redox activity of −OH$_a$ groups on CT samples was observed in a previous work by the authors by means of the Folin and Ciocalteau test.[24]

Interestingly, there is a high density of −OH groups also on the samples containing silver: these functional groups are not exhausted in the reaction with silver. The amount of residual −OH is related to the time of insertion of the additive and silver precursor in the process: the sooner they are added in the solution, the lower is the amount of total residual −OH on the surface, which can be represented by the ratio of the OH

Table 2. Atomic percentage of the elements detected by XPS on the surface of the treated samples. Sample CT is reported as reference.

Elements	CT	CT_Ad + Ag (0.005 M)_T1	CT_Ad + Ag (0.005 M)_T2	CT_Ad + Ag (0.005 M)_T3	CT_Ad + Ag (0.00 1 M)_T2
O	60.7	41.65 ± 3.46	49.35 ± 0.46	45.90 ± 5.80	47.97 ± 0.4
C	20.7	34.60 ± 4.95	31.10 ± 0.10	31.45 ± 1.90	38.05 ± 0.18
Ti	16.2	10.55 ± 2.90	13.30 ± 0.35	12.10 ± 1.70	12.49 ± 0.38
Ag	–	12.90 ± 0.10	5.85 ± 0.20	10.60 ± 5.52	1.49 ± 0.01
Others	2.3	–	–	–	–

**ADVANCED
SCIENCE NEWS**

www.advancedsciencenews.com

**ADVANCED
ENGINEERING
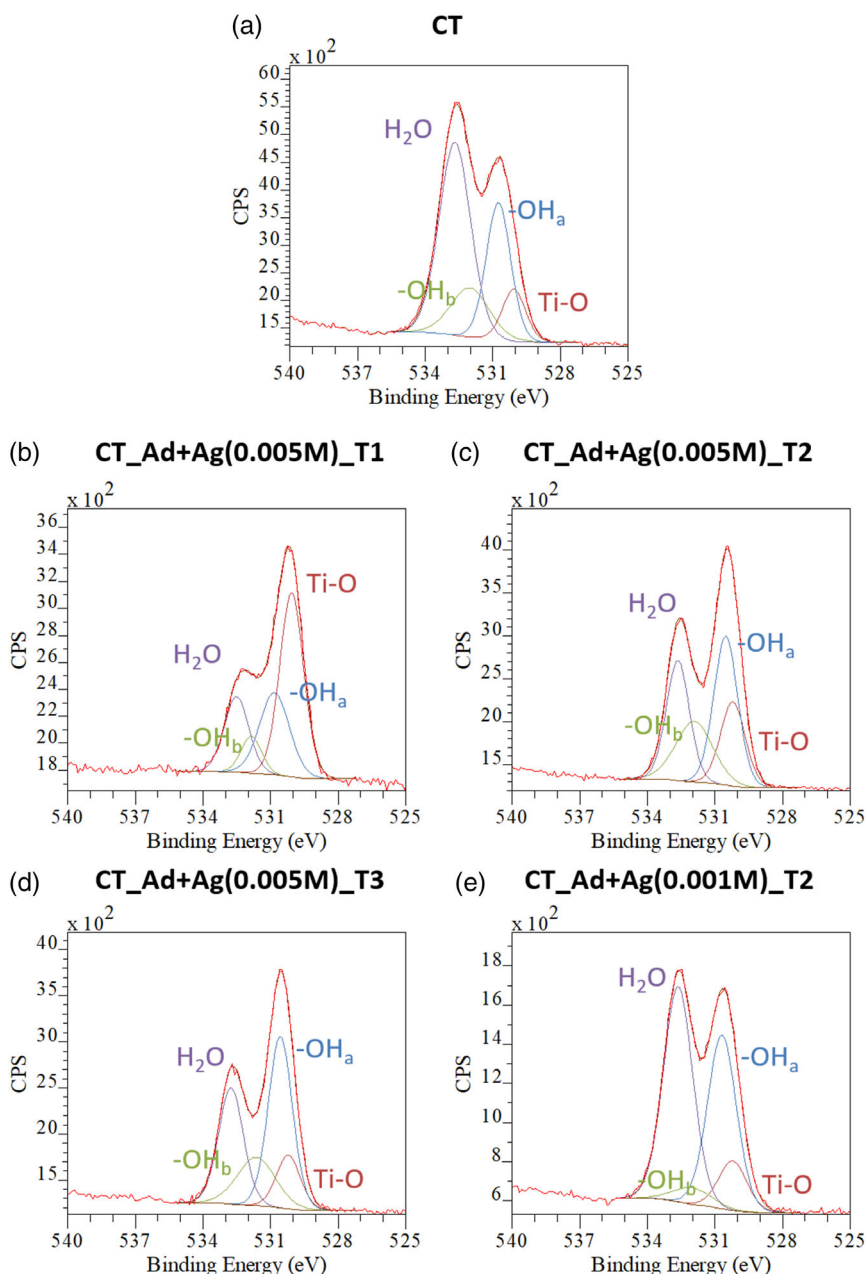MATERIALS**

www.aem-journal.com

Figure 2. XPS profile fitting of the oxygen region of the samples: a) CT, b) CT_Ad + Ag (0.005 M)_T1, c) CT_Ad + Ag (0.005 M)_T2, and d) CT_Ad + Ag (0.005 M)_T3.

versus TiO concentration. This value increases from 0.7 for CT_Ad + Ag (0.005 M)_T1, to 2.8, and 4.6 for CT_Ad + Ag (0.005 M)_T2 and CT_Ad + Ag (0.005 M)_T3, respectively. Similar considerations can be made with respect to the concentration of silver. In fact, the OH/TiO ratio for CT_Ad + Ag (0.001 M)_T2 is 4.0, which is also closer to the ratio of CT samples, 4.3. This corroborates the hypothesis that hydroxyls actively participate to the reduction of silver NPs. The amount of adsorbed water varies on the different surfaces, and it is larger on the samples with a higher concentration of −OH. The presence of hydroxyl groups on the final surfaces is important

because they have a role in the bioactive behavior in contact with the biological fluids and in the precipitation of hydroxyapatite.[13] A high density of −OH groups can be also beneficial for the cytocompatibility and cell response of the titanium surface.[25]

In **Figure 3**, the spectra of the silver region are visible. The profile fitting of CT was not performed in this region because no Ag was detected on this sample, as expected. Two peaks are evident in the spectrum of the sample CT_Ad + Ag (0.005 M)_T1, which are due to four different contributes. The peaks at about 368.5 and 374.5 eV are due to the presence of the metallic silver as nanoparticles.[26,27] The two peaks at about
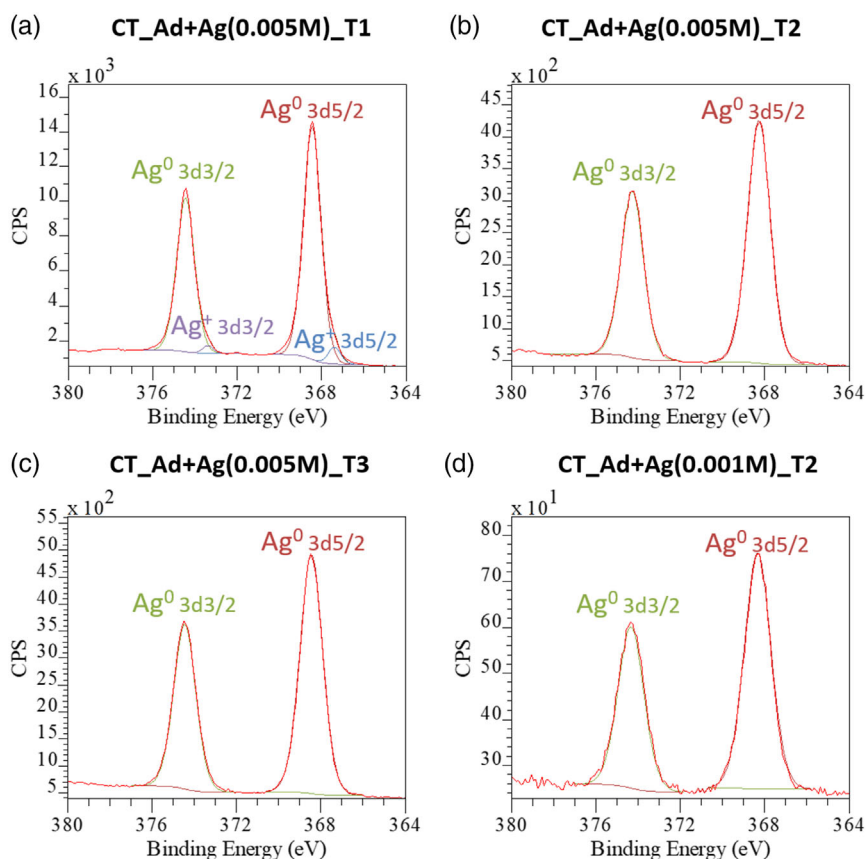
ADVANCED
SCIENCE NEWS
www.advancedsciencenews.com

ADVANCED
ENGINEERING
MATERIALS
www.aem-journal.com

Figure 3. XPS profile fitting of the silver region of the samples: a) CT_Ad + Ag (0.005 M)_T1, b) CT_Ad + Ag (0.005 M)_T2, c) CT_Ad + Ag (0.005 M)_T3, and d) CT_Ad + Ag (0.001 M)_T2.

367.8 and 373.8 eV are due to the presence of silver ions embedded into the titanium oxide or to a silver oxide layer covering the nanoparticles; they involve about 6% of the area of the silver peaks.[28] The presence of silver in an oxide state in the case of CT_Ad + Ag (0.005 M)_T1 can be related to the longer contact with the hydrogen peroxide solution. On the samples CT_Ad + Ag (0.005 M)_T2 and CT_Ad + Ag (0.005 M)_T3, there are only the two peaks due to metallic silver.[27,29] According to the XPS and FESEM results, it can be concluded that the T2 and T3 protocols induce the formation on the outermost layer of the samples of silver metal nanoparticles so small to be not observable by FESEM. The presence of silver nanoparticles on CT_Ad + Ag (0.005 M)_T1 observed by FESEM is confirmed by XPS with the additional information of a limited oxidation.

2.2. Cross-Section Characterization

The transmission electron microscopy (TEM) and scanning transmission electron microscopy (STEM)–EDS analyses were performed using the lamellae cut perpendicularly to the surface of the investigated samples CT_Ad + Ag (0.005 M)_T1, CT_Ad + Ag(0.005 M)_T2, and CT_Ad + Ag (0.005 M)_T3 to investigate the cross-section microstructure and chemical composition, in particular distribution of the silver nanoparticles across the thickness of the titanium oxide layer using different protocols. The TEM images of the cross sections of the T1–T3 samples are shown in **Figure 4**.

Observing the sample cross section, a difference in the thickness of the oxide layer is clearly visible. The thickness of the oxide layer is around 170 nm on the sample CT_Ad + Ag (0.005 M)_T1, it is around 200 nm on CT_Ad + Ag (0.005 M)_T2, and it is around 240 nm on CT_Ad + Ag (0.005 M)_T3. This difference in the oxide thickness is correlated with the time of addition of the silver precursor and additives in the preparation of the surfaces. The sooner the silver precursor is added during the growth of the oxide layer, the thinner the final layer. This phenomenon can be explained considering that in the presence of silver, both the chemical reactions of silver reduction and titanium oxidation occur at the material surface and in these conditions the growing rate of the titanium oxide layer is slowed down, as previously observed by the authors.[10] It is also evident that the oxide layer preferentially grows along the grain boundaries of titanium going in depth below the surface.

There are large nanoparticles, above 50 nm in diameter, which are generally not in the outermost layer, but distributed along the thickness of the oxide layer and at the boundary with the underlying titanium alloy. These large nanoparticles are more abundant on the samples in which the silver precursor was added later on, when the growth of the oxide layer already occurred (CT_Ad + Ag (0.005 M)_T2 and CT_Ad + Ag (0.005 M)_T3).
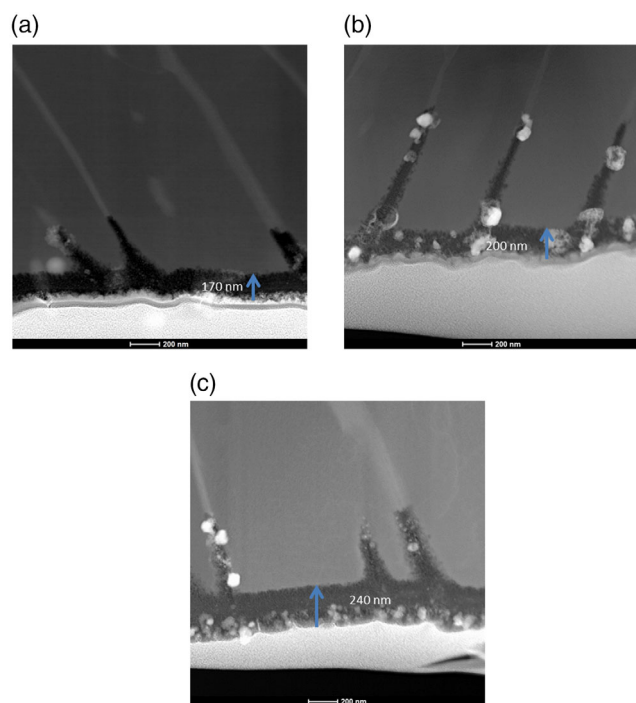
Figure 4. TEM images of the cross section of a) CT_Ad + Ag (0.005 M)_T1, b) CT_Ad + Ag (0.005 M)_T2, and c) CT_Ad + Ag (0.005 M)_T3 at the magnification of 40 k×. The outermost surface layer is downward facing.

It means that the nanoporosity of the oxide layer let the silver atoms diffuse across the oxide layer, allowing the formation of the silver nanoparticles also inside the oxide layer already grown and at the interface with the metal alloy. More detailed TEM images taken at higher magnification of these samples are reported in **Figure 5**.

In Figure 5, the presence of both very fine (not explicitly measurable) and of large (above 50 nm in diameter) nanoparticles are visible on the different samples with various distribution. On the sample CT_Ad + Ag (0.005 M)_T1, the nanoparticles are very small with a higher density on the outermost layer, as well visible in the image taken at 115 k×. On the sample CT_Ad + Ag (0.005 M)_T2, larger nanoparticles are observable preferentially in the middle of the oxide layer and along the grain boundaries, whereas on the sample CT_Ad + Ag (0.005 M)_T3 the nanoparticles are accumulated just below the outermost surface with few large particles along the grain boundaries. The presence of subsurface particles in the case of CT_Ad + Ag (0.005 M)_T3 can explain the high standard deviation of the XPS survey results on this sample, whereas the distribution of the nanoparticles of CT_Ad + Ag (0.005 M)_T1 agrees with the higher silver content detected by the XPS survey analysis.

Figure 6 shows the STEM–high-angle-annular dark-field (HAADF)–EDS distribution maps of the selected chemical elements (Ti, O, and Ag) acquired on the T1–T3 sample cross sections. The findings based on the EDS analysis are consisted with the conclusion drawn from the TEM images evidencing that the presence of silver is widespread and distributed across all the

thickness of the oxide layer on all the samples, even if the distribution of the nanoparticles is different case by case.

These analyses suggest that the different protocols with different times of addition of the silver precursor and additives allow to obtain different surface oxide layers. The formation of a thicker oxide layer on CT_Ad + Ag (0.005 M)_T2 and CT_Ad + Ag (0.005 M)_T3 is of interest in view of a higher corrosion resistance of the surface. The sponge-like structure of the titanium oxide allows the diffusion of silver atoms and the formation of silver nanoparticles deeply below the outermost layer, even more if the silver addition occurs when the oxide layer has been already partially grown. In the case of the addition of the silver precursor and additives later on in the oxidation process (CT_Ad + Ag (0.005 M)_T2 and CT_Ad + Ag (0.005 M)_T3), the absence of accumulation of nanoparticles on the outermost layer is of interest to avoid the release of nanoparticles from the surface, as it can occur in the case of CT_Ad + Ag (0.005 M)_T1, and to get a prolonged antibacterial action that is the aim of this research.

2.3. Silver-Ion Release

In **Figure 7**, the silver-ion release over time of the samples is reported.

The samples have a maximum release after 24 h. For all the samples, the silver release lasts up to 14 days (336 h) and since 1 up to 7 days (168 h), it is higher for the samples treated with the protocol T2 and T3. The standard deviation of the samples prepared with a higher concentration of the silver precursor (0.005 M) is low indicating good reproducibility. No release was detected by any sample after 28 days of soaking in water. The addition of the additives and silver precursor after the first growth of the oxide layer, such as it occurs in the protocols T2 and T3, leads to sustaining the silver release for a longer time with respect to T1. This is of interest for a prolonged antibacterial action of the surface and agrees with the TEM observations.

The graph of the cumulative silver release is reported in **Figure 8**. The concentration 1 mg L^{-1} that is the MIC of silver on many bacteria can be considered as a reference for the antibacterial action. On the other side, the LC$_{100}$ for fibroblasts (concentration at which 100% of the cells die) is the reference for cytocompatibility, and it was found in literature to be 60 mg L^{-1}.[4,5,30] The cumulative release by the investigated samples is higher for the samples treated with the protocol T2 and it is 0.85 mg L^{-1} close to the MIC value and lower than the cytotoxicity threshold. It can be concluded that the silver release lasts until 14 days with an amount of silver suitable for antibacterial purpose and it is higher and more prolonged for the protocols T2 and T3.

As expected, the release from CT_Ad + Ag (0.001 M)_T2 is significantly lower than the other samples (Figure 7), in particular after 3 and 24 h. A small release was observed also after 168 h. No release was detected after 14 days, earlier than the samples treated with a higher silver concentration. The cumulative release in Figure 10 shows that all the silver has been released within the first 7 days of soaking using this protocol. Because of this fact, the release was not continued till 42 days. The lower release is
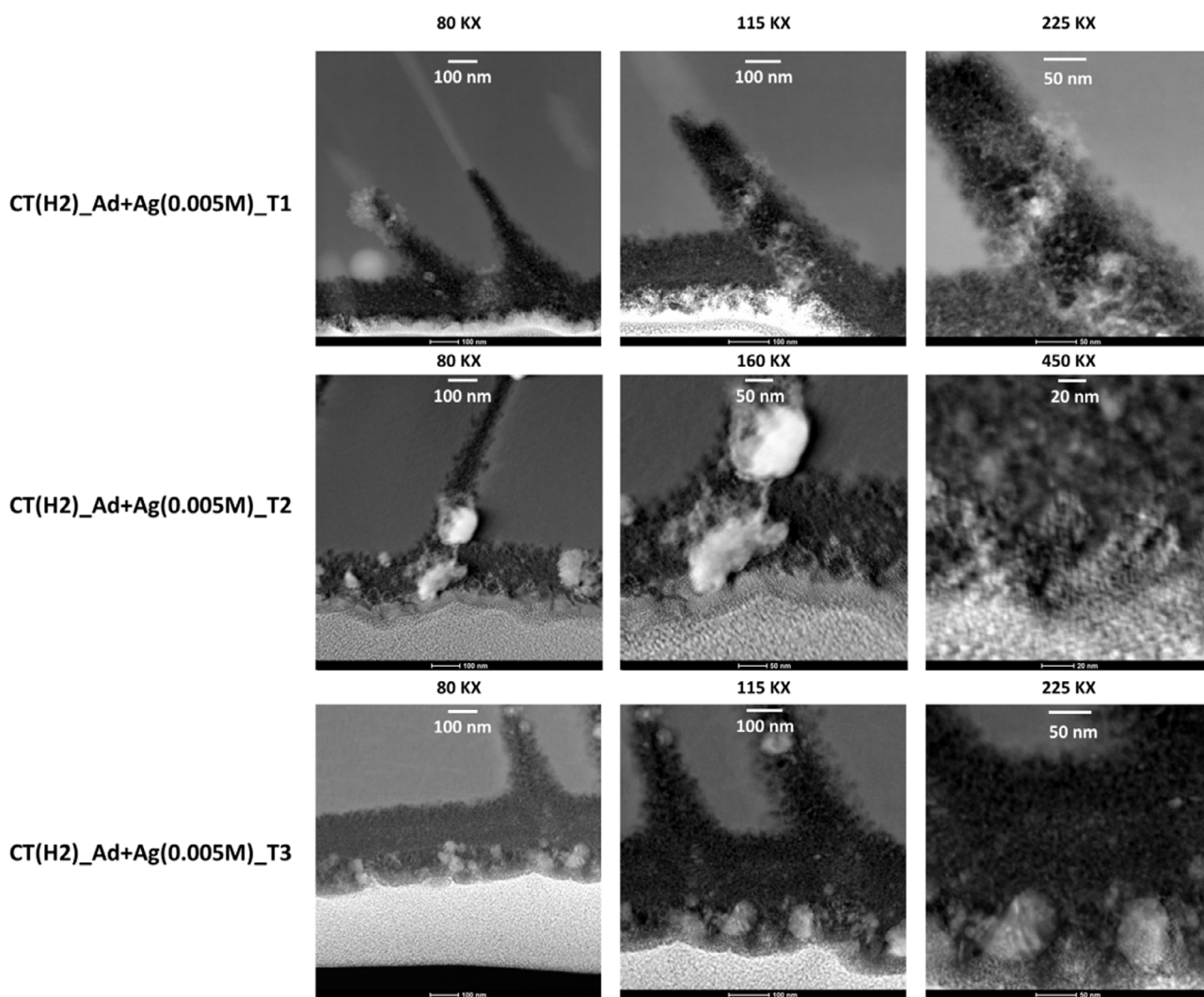
Figure 5. Enlarged TEM images of the samples cross section CT_Ad + Ag (0.005 M)_T1, CT_Ad + Ag (0.005 M)_T2, and CT_Ad + Ag (0.005 M)_T3. The outermost surface layer is downward facing.

consistent with the overall lower amount of silver on the surface of CT_Ad + Ag (0.001 M)_T2 samples detected by XPS and EDS.

At the end of the chemical and physical characterization, it can be concluded that the T2 and T3 protocols are the most interesting because of the thicker oxide layer (TEM), presence of silver as metal nanoparticles without accumulation on the outermost layer (FESEM, TEM, and XPS), and the higher and more prolonged silver release. The T2 protocol is selected as the most interesting considering the lower amount of silver in the outermost layer (XPS) even if the average amount of silver across the overall oxide layer is comparable with the other samples (EDS): lower risk of cytotoxicity can be expected. On the other side, it is of interest to compare CT_Ad + Ag (0.005 M)_T2 and CT_Ad + Ag (0.001 M)_T2 because of their significant different amounts of silver both on the surface (EDS and XPS) and released. It is noteworthy that the amount of silver ions released by both types of surfaces falls in the concentration range suitable for being antibacterial but not cytotoxic, which is between $0.1 \, \mu g \, L^{-1}$ and $10 \, mg \, L^{-1}$.[31,32] According to these observations, these two samples were characterized through the biological tests.

2.4. Antibacterial Properties Evaluation

Here, according to the possible application in Orthopaedics of the proposed coating aimed at implantable metallic devices, *S. aureus* was selected as target pathogen due its frequent involvement in joint infections.[33] Moreover, the possible specimens' inhibition effect was tested toward both the planktonic and biofilm populations, representative of the floating and of the surface-adherent components of the bacterial infection, respectively. Therefore, the focus was directed toward the different silver amount due to the preparation procedure in view of the ability to prevent biofilm adhesion onto the surface as well as to reduce the number of viable floating bacteria propagating the infection systemically. Results are reported in Figure 11 (planktonic) and Figure 12 (biofilm).
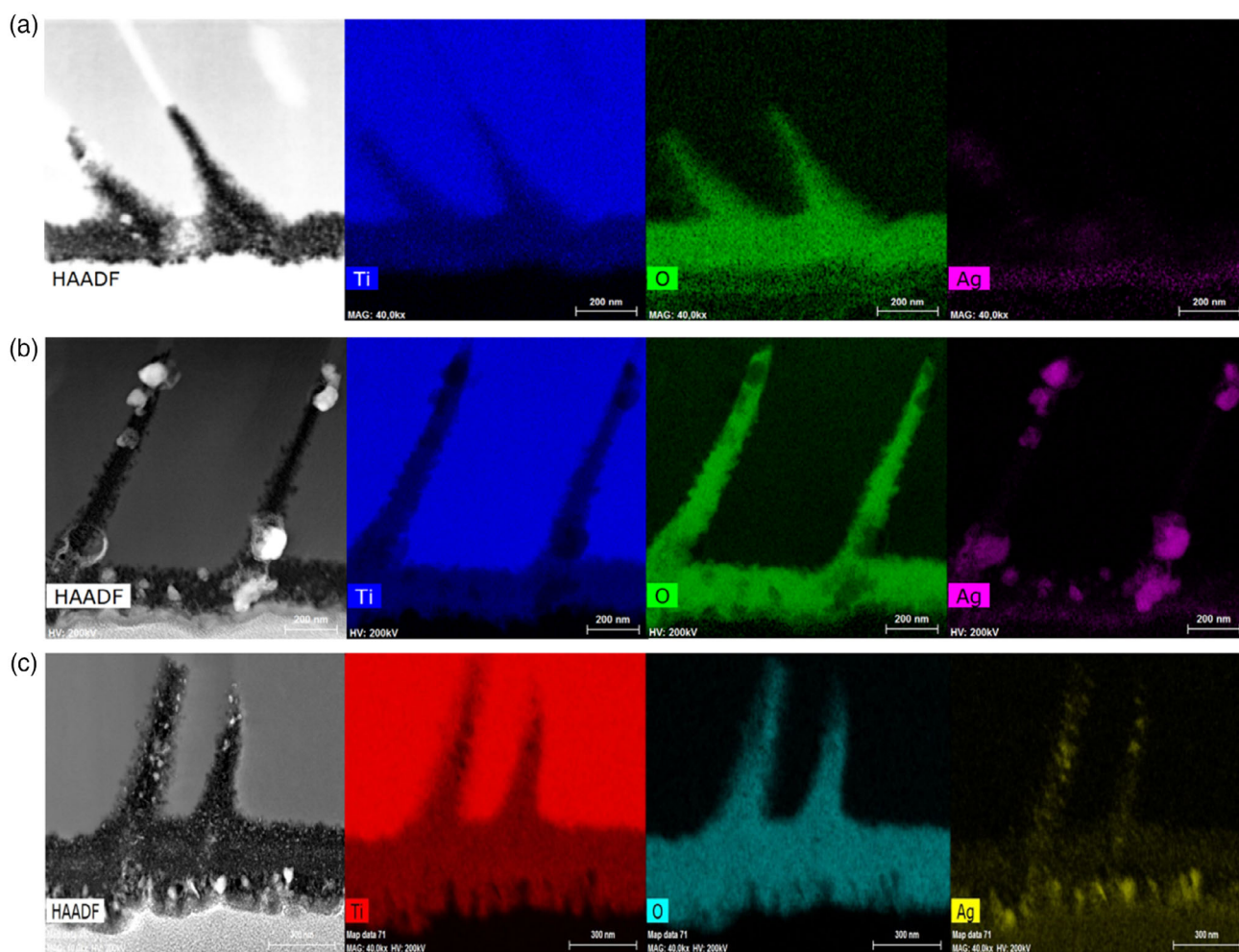
Figure 6. STEM_EDS maps of the cross section of the samples: a) CT_Ad + Ag (0.005 M)_T1, b) CT_Ad + Ag (0.005 M)_T2, and c) CT_Ad + Ag (0.005 M)_T1 at the magnification of 40 k×. The outermost surface layer is downward facing.
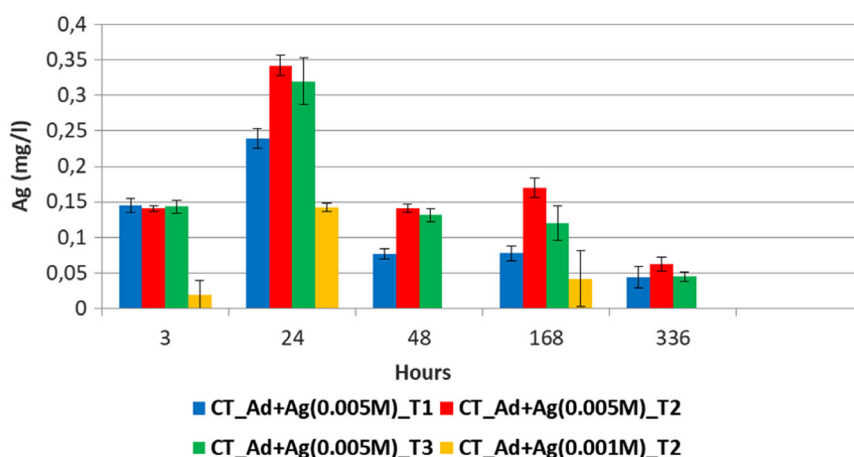

Figure 7. Silver-ion release in water over time by the treated samples.

In general, only the sample prepared with the higher concentration of $AgNO_3$ (named CT_Ad + Ag (0.005 M)_T2) showed a strong antibacterial activity toward the floating planktonic cells (**Figure 9**). In fact, the viability of the planktonic counterpart is early, significantly decreased at 2, 4, and 6 h in comparison with both polystyrene control and mirror-polished uncoated
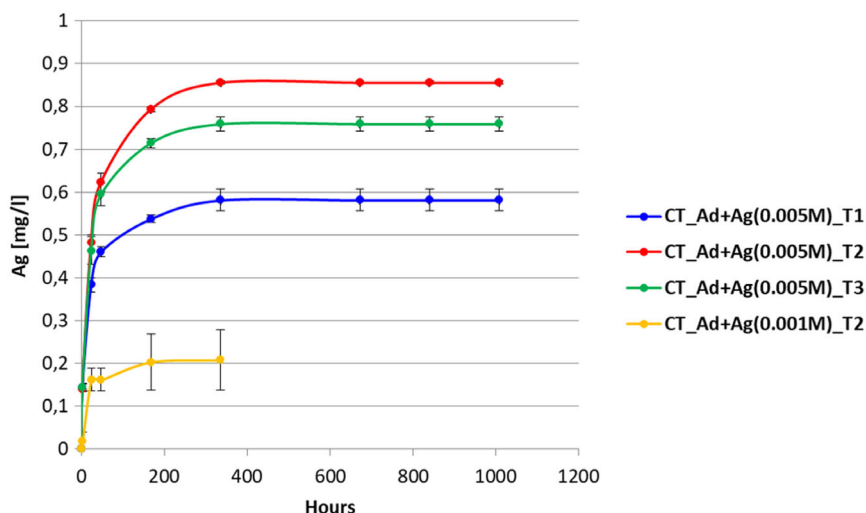
Figure 8. Cumulative silver-ion release by the treated surfaces over time (the curve of CT_Ad + Ag (0.00 1 M)_T2 was interrupted after 336 since no more silver was released later).
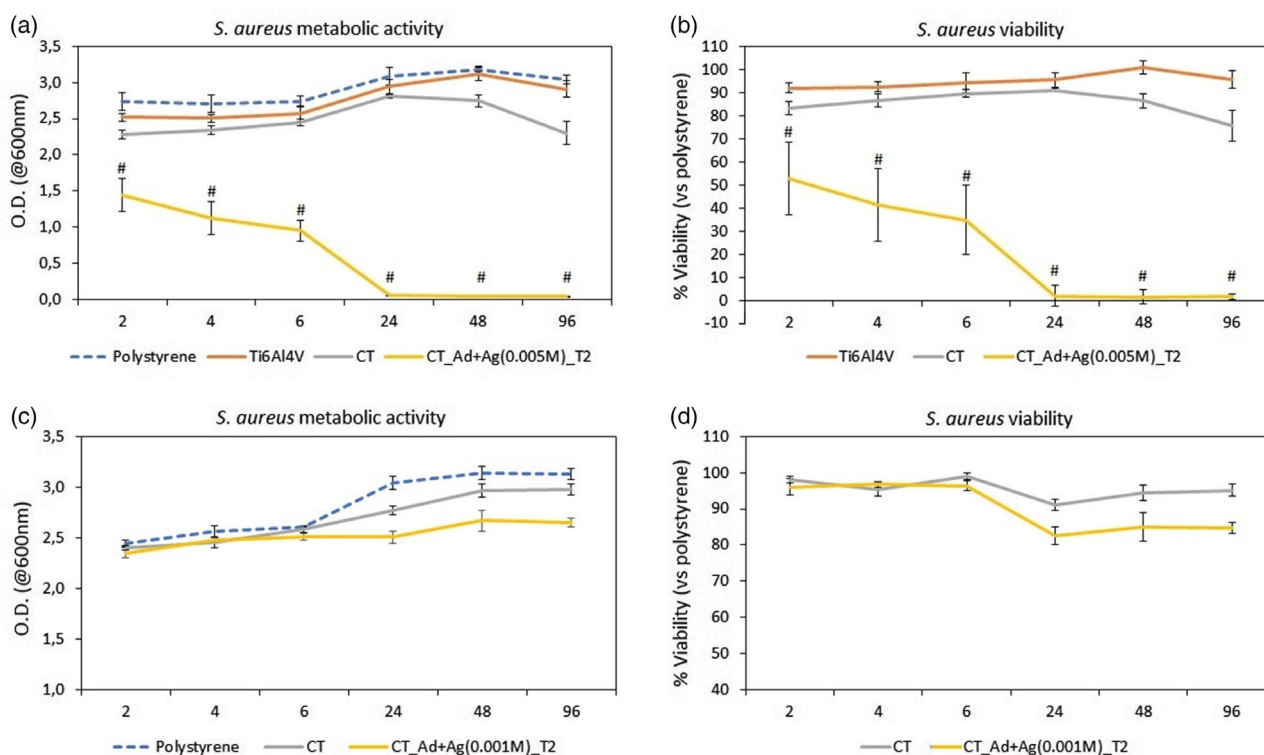

Figure 9. *S. aureus* planktonic cells metabolic activity and viability (%) after 2, 4, 6, 24, and 48 h in contact with a,b) CT_Ad + Ag (0.005 M)_T2 and c,d) CT_Ad + Ag (0.00 1 M)_T2. Results are summarized as OD and percent viability versus polystyrene in function of time. Bars represent means ± standard deviations, replicates $n = 3$.

Ti_6Al_4V ($p < 0.05$, indicated by #), whereas after 24 h a $> 97\%$ of metabolic reduction was observed, thus, suggesting for an almost complete eradication of viable bacteria. Accordingly, the following time points (48 and 96 h) confirmed that all the majority of the floating cells were previously killed by the Ag^+ ions released from CT_Ad + Ag (0.005 M)_T2. Conversely, a nonsignificant reduction was obtained for the bare CT samples and the CT_Ad + Ag (0.001 M)_T2, if compared with the polished Ti_6Al_4V samples and with the polystyrene control ($p > 0.05$). In absence of silver, a slight antimicrofouling action (passive antiadhesive ability) of the CT layer has been already previously reported by the authors and it can be

ADVANCED
SCIENCE NEWS
www.advancedsciencenews.com

ADVANCED
ENGINEERING
MATERIALS
www.aem-journal.com

ascribed to the nanotopography and to the high hydroxylation degree.[14]

According to the obtained results, here it is reasonable that in the applied experimental conditions CT_Ad + Ag (0.005 M)_T2 specimens are able to release an effective amount of Ag$^+$ ions to determine floating bacteria killing within 24 h (Figure 9), in agreement with the observed silver release.

Similar results were obtained by evaluating samples' activity toward the formation of biofilm by *S. aureus* (Figure 9). The samples prepared with a high concentration of AgNO$_3$ (CT_Ad + Ag (0.005 M)_T2) were effective in reducing biofilm viability even at early time points 2, 4, and 6 h ($p < 0.05$ vs control, indicated by #) and no living bacteria were metabolically active and were further detected after 24, 48, and 96 h. Different from the planktonic studies, when the surface-adherent biofilm was studied, the CT_Ad + Ag (0.001 M)_T2 specimens reported an antibacterial effect after 24 h of direct contact that was significant in comparison with the control ($p < 0.05$, indicated by #). So, it can be hypothesized that due to the lower Ag amount exposed to the surface, they required more time to be effective in comparison with CT_Ad + Ag (0.005 M)_T2, but such ion concentration can be effective in counteracting the infection in a longer (24 h) period. In fact, the Ag-exploited killing effect is the same onto both the materials and it is well known that due to the formation of irreversible pores on the membrane, direct DNA damage impairing the replication and generation of oxidative stress occurs.[34] So, the observed differences in terms of velocity and killing ratio can be logically ascribed to the silver amount rather than to different biochemical mechanisms, thus, confirming a dose-dependent effect.

Finally, fluorescence live/dead assay performed onto biofilm grown for 96 h (**Figure 10**) confirmed the results obtained by the metabolic assay showing the presence of living bacteria in the 3D aggregates biofilm shape onto untreated TI$_6$Al$_4$V mirror-polished surfaces (upper panel, stained in green), whereas only few single random dead ones are noticed onto CT_Ad + Ag (0.001 M)_T2 and CT_Ad + Ag (0.005 M)_T2 surfaces (middle and lower panel, stained in red).

2.5. Cytocompatibility

Cytocompatibility of the samples CT_Ad + Ag (0.005 M)_T2 and CT_Ad + Ag (0.001 M)_T2 is evaluated toward human osteoblasts progenitor (hFOB) after 24, 48, and 72 h of direct seeding on. Because of the possibility to apply the developed materials as implantable devices, those cells were selected as representative of the progenitor cells deputed for the tissue healing and ingrowth around the implant migrating from the neighbor physiological tissue due to the tissue injury. The results are reported in **Figure 11**. Unfortunately, the presence of silver on CT_Ad + Ag (0.005 M)_T2 introduced a marked toxic effect in the case of CT_Ad + Ag(0.005 M)_T2 that was evident after 24 h; then, the cells' viability continued to decrease after 48 and 72 h, thus, reporting significant reductions in comparison with the controls ($p < 0.05$, indicated by #). Accordingly, the cells' viability was reduced of >80% after 72 h of direct contact.
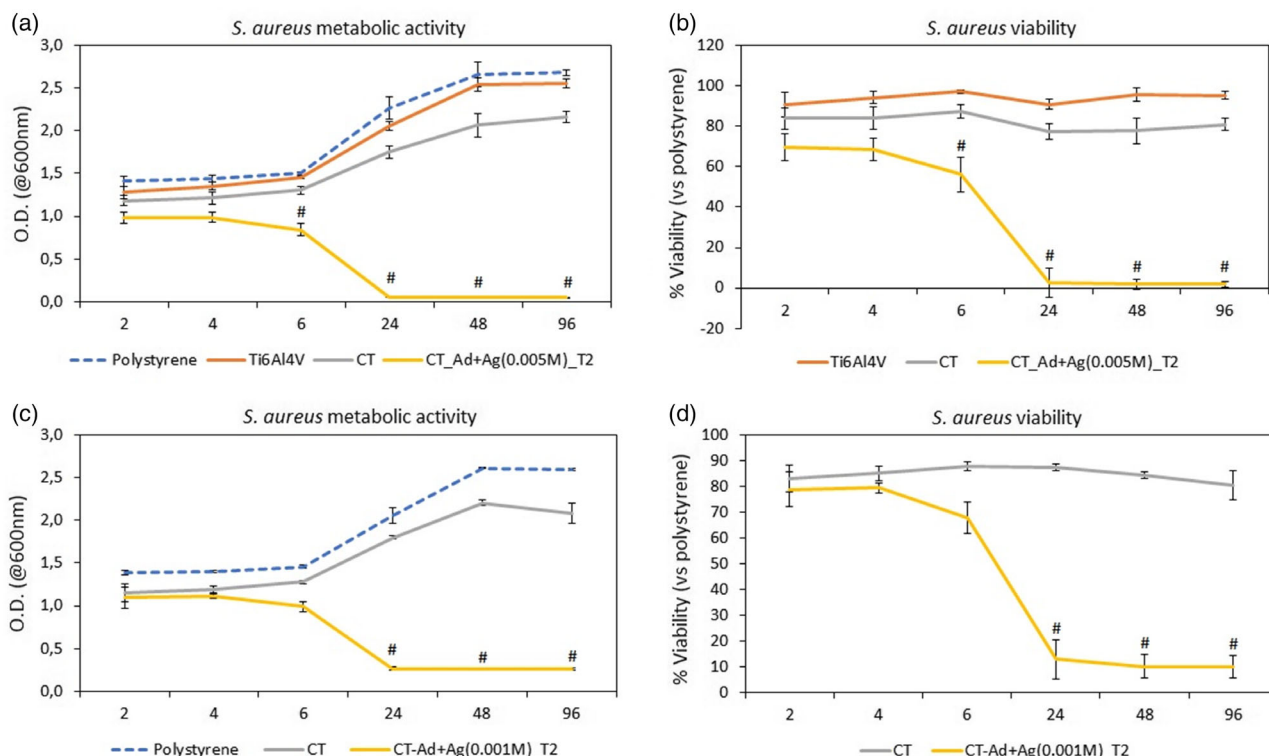

Figure 10. *S. aureus* biofilm cells metabolic activity and viability (%) after 2, 4, 6, 24, and 48 h in direct contact with a,b) CT_Ad + Ag (0.005 M)_T2 and c,d) CT_Ad + Ag (0.001 M)_T2. Results are summarized as OD and percent viability versus polystyrene in function of time. Bars represent means ± standard deviations, replicates n = 3.
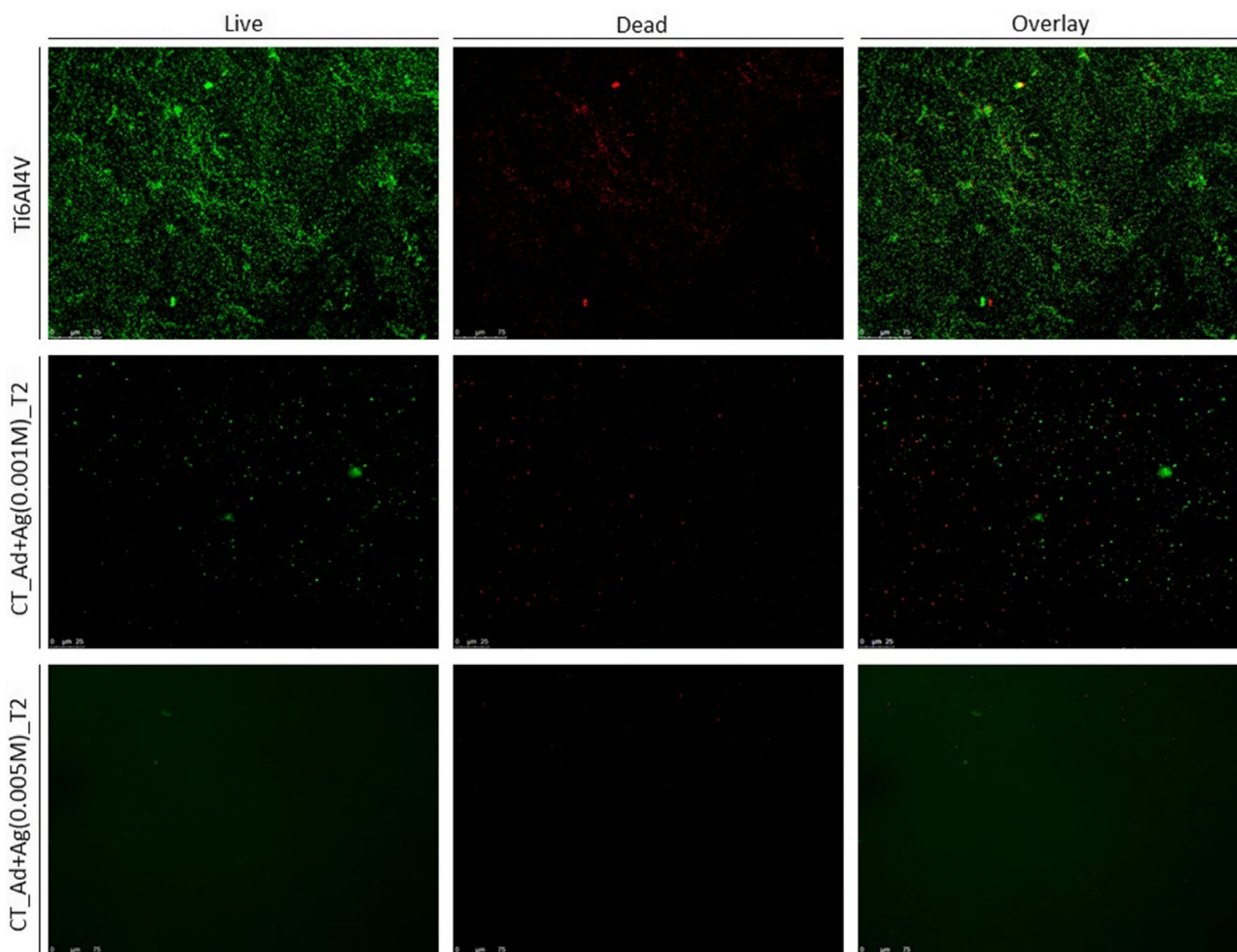
**ADVANCED
SCIENCE NEWS**

www.advancedsciencenews.com

**ADVANCED
ENGINEERING
MATERIALS**

www.aem-journal.com

Figure 11. Live/dead staining of 96 h *S. aureus* biofilm grown onto polished Ti_6Al_4V (upper panel), CT_Ad + Ag (0.00 1 M)_T2 (middle panel), and CT_Ad + Ag (0.005 M)_T2 (lower panel). Living bacteria are marked in green, whereas dead bacteria are in stained in red. Images magnification 20× and bar scale = 25 um.

These results evidenced a strong cytotoxic effect of the CT_Ad + Ag (0.005 M)_T2 specimens that were not expected by observing the amount of the released silver. However, the observed toxicity could be correlated with the direct contact of cells with the silver nanoparticles coated onto the surface, which involves different mechanisms than the released ions. The choice of opting for the direct seeding of the cells on the surface of the materials is due to the need of verifying the possibility of progenitor cells to colonize or to grow in direct contact with the surface of the implanted device. This is a condition of crucial importance in the clinical scenario to successfully promote the tissue repair. In line with the previous literature, a similar effect was previously reported by Sussman et al. (2015);[35] they compared the cytotoxicity of plastic surfaces coated with silver nanoparticles at different concentrations by direct (cells directly seeded onto surfaces) and indirect (a mix of stock solution and medium applied for cells cultivation) assay displaying not comparable results between the two methods. They assumed that in the case of the direct seeding of the cells, in addition to silver concentration, other

parameters are considered to play a pivotal role for cells' adaptation to the surface such as physical morphology, crystallinity, the oxidation state of Ag, the presence of other chemicals, and coordinating species.[36] On the opposite, the released Ag from the same specimens resulted as less cytotoxic probably due to the reaction or the aggregation with the proteins restrained in the cell culture media and in the serum. Therefore, a linear correlation between the released ions and the cytotoxicity was not evidenced.

The same test was then performed for the samples CT_Ad + Ag (0.001 M)_T2 and results are reported in **Figure 12**. The sample preparation with a diluted silver precursor unfortunately reported again a marked toxic effect that was observed from the first time point of 24 h; then, cells' viability still decreased after 48 and 72 h, being significantly reduced in comparison with the polystyrene control ($p < 0.05$, indicated by #). However, for those specimens, the percentage of viable cells after 72 h was ≈50%, thus, the observed toxicity was marked lower than the previous results reported by CT_Ad + Ag
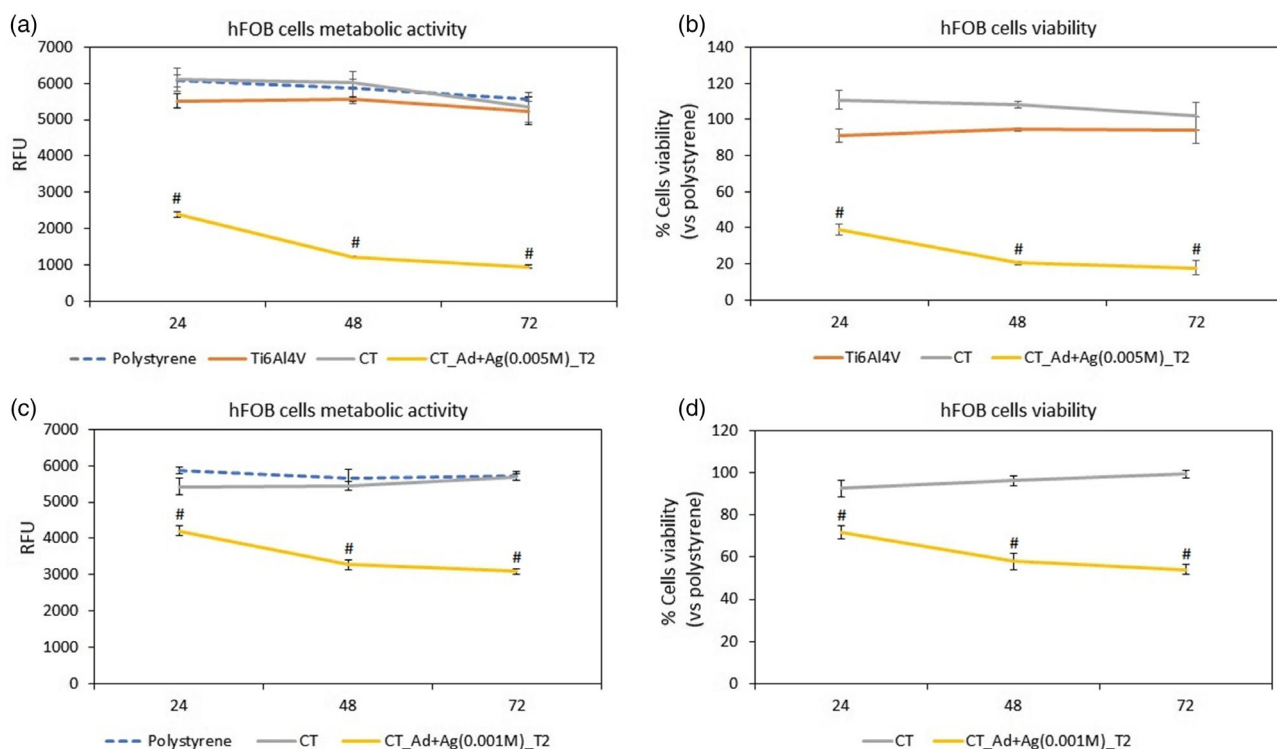
**ADVANCED
SCIENCE NEWS**

www.advancedsciencenews.com

**ADVANCED
ENGINEERING
MATERIALS**

www.aem-journal.com

Figure 12. Osteoblasts progenitor hFOB cells viability at 24, 48, and 72 h on a,b) CT_Ad + Ag (0.005 M)_T2 and c,d) CT_Ad + Ag (0.00 1 M)_T2. Results are summarized as a,c) O.D. and b,d) percent viability versus polystyrene in function of time. Bars represent standard deviations.

(0.005 M)_T2; accordingly, in addition to the previously discussed factors influencing cells' adaptation to the surface, a dose-dependent toxicity due to the Ag amount was observed as a confirmation of the previous literature.[37]

However, taking into account the strong antibacterial effect demonstrated by the CT_Ad + Ag (0.001 M)_T2 specimens toward the bacterial biofilm colonizing implant surface and the possibility to preserve half of the cells deputed for self-healing, this is an interesting result even if it must be underlined that cytotoxicity can occur in the presence of small silver nanoparticles on the surface, even if the released amount of silver is well below the toxic threshold usually described in the literature.

3. Conclusion

This research work was devoted to the in situ reduction of silver nanoparticles on the surface of the titanium alloy Ti_6Al_4V during the growth of a nanostructured layer of titanium oxide which is bioactive and suitable for bone contact applications. The developments of three different protocols which involve the addition of the additives and silver precursor at different times of the oxidation process were investigated using two different concentrations of the silver precursor. Reproducible samples with nanoparticles exposed on the surface are obtained (FESEM, EDS, and XPS); the nanoparticles are smaller when the silver precursor is added later during the chemical treatment. The TEM and STEM images of the sample cross sections showed a higher density of nanoparticles on the surface if the silver precursor is added earlier and a

distribution of the nanoparticles across all the thickness of the oxide in the other cases. The silver release in water is higher in the case of the use of a more concentrated silver precursor during the preparation and more prolonged when the precursor is added later. The preparation with a concentrated silver precursor allows to strongly reduce the viability of the floating planktonic bacteria as well as to prevent biofilm formation; however, these samples were also highly cytotoxic. The effects on planktonic bacteria are lower if a diluted silver precursor is used, but the effects on preventing biofilm colonization remain strong, whereas the cytotoxicity was reduced till 50%. These results evidence that a balance between antibacterial action and cytocompatibility is not easy to be found in the case of titanium surfaces with very small silver nanoparticles and that the silver amount is most likely not the only factor influencing the biological properties.

4. Experimental Section

Preparation of the Ti_6Al_4V Substrates: The samples were slices 2-mm thick and 10 mm in diameter of Ti_6Al_4V alloy (ASTM B348, Gr5, Titanium Consulting and Trading).

They were polished with abrasive SiC papers (up to 4000 grit) and then washed in an ultrasonic bath once in acetone for 5 min and twice in ultrapure water for 10 min. After washing, the samples were air dried at room temperature under a laminar flow hood. These samples were used as control references when needed.

Surface Chemical Treatment with In Situ Reduction of the Silver Nanoparticles: The samples were treated with a chemical treatment

previously developed and patented by the authors[38] to obtain a bioactive surface oxide layer with silver nanoparticles embedded in it. The chemical treatment consisted of etching with diluted hydrofluoric acid to remove the native oxide layer and a controlled oxidation of the surface in hydrogen peroxide in a thermostatic bath under shaking as previously detailed.[9,10] The formation of the silver nanoparticles occured through an in situ reduction of an ionic precursor during the surface chemical treatment of oxidation in hydrogen peroxide as detailed.[9,38] Three protocols (named T1, T2, and T3) were developed in this research by adding the silver precursor and additives at different times of the oxide growth during the treatment in hydrogen peroxide in the beginning of the oxidation treatment of the samples (T1), after half of the treatment time (T2, 1 h), or at two-thirds of the treatment time (1 h and 20 min). The aim was to control the formation and distribution of the silver nanoparticles within the surface oxide layer.

The used additives were GA (97.5–102.5% (titration), G7384 Sigma Aldrich) and PVA (average M_w 13 000–23 000, 98% hydrolyzed, 348 406 Sigma Aldrich). The aim of the additives was to reduce and to stabilize a high number of nanoparticles avoiding the formation of aggregates. A solution of GA 1 mg mL^{-1} and a solution of PVA 1 mg mL^{-1} in ultrapure water were prepared 1 h before each sample preparation. Then, these solutions were added to the hydrogen peroxide solution to obtain a final concentration of GA of at about 0.1 and of 0.01 g L^{-1} of PVA, as reported.[9] The silver precursor used was silver nitrate (AgNO$_3$, PA-ACS-ISO 131459, 1611, Panreac). A solution 1 M of silver nitrate in ultrapure water (5 mL of water + 0.849 g × AgNO$_3$) was prepared and added to the hydrogen peroxide solution, immediately after the additives, to obtain a final concentration of AgNO$_3$ of 0.005 M. In a second stage of the research, the concentration of silver nitrate in the hydrogen peroxide solution was reduced to 0.001 M. In this case, only the T2 condition was tested according to the obtained results. As reference, samples chemically treated without the addition neither of silver precursor or additives were also prepared.

After the chemical treatment, the samples were rinsed in ultrapure water and air dried under a laminar flow hood.

The procedure used to treat the samples is schematized in **Figure 13** and the nomenclature for each kind of sample is reported in **Table 3**.

Surface Characterization: FESEM (SUPRATM 40, Zeiss) equipped with EDS was employed to investigate the surface morphology of the samples. An area of 5400 µm^2 was chemically analyzed.

Table 3. Nomenclature of the samples and surface treatments.

Name	Description
Ti$_6$Al$_4$V	Polishing
CT	Polishing; chemical treatment in HF (hydrofluoric acid, chemical formula); chemical treatment in H$_2$O$_2$ with no addition of silver precursor and additives
CT_Ad + Ag (0.005 M)_T1	Polishing; chemical treatment in HF; chemical treatment in H$_2$O$_2$ with addition of silver precursor and additives at T1; AgNO$_3$ concentration of 0.005 M
CT_Ad + Ag (0.005 M)_T2	Polishing; chemical treatment in HF; chemical treatment in H$_2$O$_2$ with addition of silver precursor and additives at T2; AgNO$_3$ concentration of 0.005 M
CT_Ad + Ag (0.005 M)_T3	Polishing; chemical treatment in HF; chemical treatment in H$_2$O$_2$ with addition of silver precursor and additives at T3; AgNO$_3$ concentration of 0.005 M
CT_Ad + Ag (0.00 1 M)_T2	Polishing; chemical treatment in HF; chemical treatment in H$_2$O$_2$ with addition of silver precursor and additives at T2; AgNO$_3$ concentration of 0.001 M

The surface chemical composition and chemical state of the elements were investigated also by means of XPS (PHI 5000 Versa probe, physical electronics) in survey and high-resolution mode for carbon.

Cross-Section Characterization: Characterization of the morphology, microstructure, and chemical composition of the investigated samples, in particular, the distribution, shape, and dimension of the silver nanoparticles, was performed by TEM and STEM as well as STEM–EDS by a probe-corrected Titan G2 60-300 electron microscope (FEI) equipped with a ChemiSTEM system.[39] The STEM imaging, acquired using HAADF detector, and EDS mapping were used for characterization of the samples' nanostructure and chemical composition.

For these investigations, ultrathin specimens (lamellae) were prepared directly from selected areas of the oxidized samples via the focused ion beam (FIB) technique using the NEON CrossBeam 40EsB (Zeiss). The lamellae, cut perpendicularly to the surface of the investigated samples,
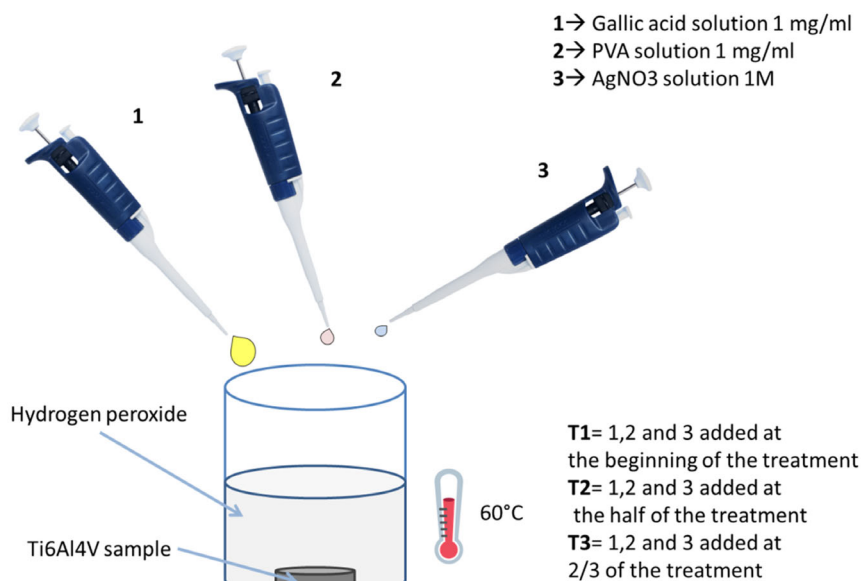

1→ Gallic acid solution 1 mg/ml
2→ PVA solution 1 mg/ml
3→ AgNO3 solution 1M

Hydrogen peroxide

60°C

Ti6Al4V sample

T1= 1,2 and 3 added at the beginning of the treatment
T2= 1,2 and 3 added at the half of the treatment
T3= 1,2 and 3 added at 2/3 of the treatment

Figure 13. Scheme of the procedure for the sample preparation.

**ADVANCED
SCIENCE NEWS**

www.advancedsciencenews.com

**ADVANCED
ENGINEERING
MATERIALS**

www.aem-journal.com

were prepared by sputtering their surfaces with Ga^+ ions emitted from a source with liquid metal. First, the Pt protective layer was deposited on the sample top surface, to prevent the occurrence of the curtaining effect, that is, the irregular removal of material. The final thinning was performed after mounting the lamella in a copper grid. This method minimizes the occurrence of artefacts during sample preparation and can be used to obtain thin, clean lamellae of uniform thickness, suitable for TEM/STEM imaging and quantitative EDS analyses.

Silver Release: The amount of silver released into ultrapure water from the surfaces of the treated samples was determined by means of a photometer for silver analysis (HI 93737, Hanna Instruments, detection range 0.000–1.000 ± 0.005 mg L^{-1}). Each sample was soaked in 25 mL of ultrapure water at 37 °C. After 3 h, 1, 2, 7, 14, and 28 days the solution was changed with a fresh one and analyzed for the silver content. The release test was performed in triplicate for each sample.

Biological Evaluations: Antibacterial Properties Evaluation: A single colony of a multidrug resistant (MDR) *S. aureus* (reference strain ATCC 25923, purchased from the American Type Culture Collection, Manassas, USA) from an overnight culture onto selective Mannitol Salt Agar plate (Sigma-Aldrich) was resuspended in 20 mL of Luria Bertani broth (LB, Sigma-Aldrich) and incubated at 37 °C for 18 h. After incubation, a new fresh LB tube diluted 1:10 was prepared. The new tube was incubated at 37 °C for 2 h to achieve the logarithmic growth phase. Finally, a fresh broth culture was prepared prior each experiment by diluting bacteria in LB broth until optical density (OD) resulted as 0.005 at 600 nm wavelength, corresponding to a final concentration of 1×10^5 cells mL^{-1}.[40]

Sterile specimens were placed in a 24-multiwell plate (Nunclon Delta Surface, Thermo Scientific) and submerged in 1 mL of LB medium containing 1×10^5 cells mL^{-1} prepared as previously described. The plate was incubated for 90 min at 37 °C under agitation at 120 rpm (adhesion phase). Supernatants were then extracted to remove floating planktonic cells (separation phase) and specimens gently washed three times with phosphate-buffered saline (PBS) to remove nonadherent cells.[41] Then, each specimen was rinsed with 1 mL of fresh LB medium and plate incubated for 24, 48, and 72 h at 37 °C for biofilm culture.

To assess the growth capacity of the bacterial strains after 24, 48, and 72 h of direct contact compared with that of untreated controls, bacterial viability was evaluated by the validated quantitative colorimetric metabolic 2,3-bis(2-methoxy-4-nitro-5-sulphophenyl)-5-[(phenylamino)carbonyl]-2 H-tetrazolium hydroxide assay (XTT, Sigma-Aldrich). Briefly, 20 μL of XTT solution (3 mg mL^{-1} in acetone containing 0.1 M menadione) were added to each well and plates were incubated at 37 °C for 5 h in the dark. Then, 50 μL were collected from each well and centrifuged for 2 min at 480 g to remove any debris, and the OD was evaluated using a spectrophotometer (SpectraCount, IBM) at 490 nm. Untreated Ti_6Al_4V mirror-polished specimens were considered as control.

To determine the viability of bacteria, a live/dead BacLight bacterial viability kit (Molecular Probes, Life Technologies Italia, Monza, Italy) was used. The kit includes two fluorescent nucleic acid stains SYTO9 and propidium iodide. SYTO9 penetrates and stains both viable and non-viable bacteria, whereas propidium iodide enters only damaged/dead cells and quenches SYTO9 fluorescence. For assessing viability, 1 mL of stock solution of each stain was added to 3 mL of PBS and, after mixing, the solution was distributed into the plates containing the materials' specimens and incubated at RT for 15 min in the dark. Stained biofilms were examined by a fluorescent microscope (Leica 6500, Leica Microsystems, Basel, Switzerland). Finally, the number of dead bacteria was calculated and expressed as percent of total bacteria number by ImageJ (NIH, Bethesda, USA) software.

Biological Evaluations: In Vitro Cytocompatibility Evaluation: Samples' cytocompatibility was evaluated toward hFOB-1.19 that were purchased from the American Type Culture Collection (ATCC, Manassas, USA, ATCC CRL-11372). hFOB were cultured in DMEM: Ham's F12 mixture (50:50, Sigma) supplemented with 10% fetal bovine serum, 1% antibiotics, and 0.3 mg mL^{-1} neomycin (G418 salt, Sigma). Cells were cultured at 34 °C, 5% CO_2 until 80–90% confluence, detached with trypsin–EDTA solution (Sigma), and used for experiments. Sterile specimens, prepared in clean and sterile conditions (substrates, water, and tools were

autoclaved prior use and the treatment was performed under a biological hood), were gently collected with surgical tweezers avoiding any surface impairment and seeded onto a new 24-well plate; the cells (hFOB) were seeded in a defined number (1×10^4 cells/specimen) directly onto specimens' surface and cultivated using 1 mL of fresh medium for 24, 48, and 72 h at 37 °C, 5% CO_2. Afterward, at each selected timepoint, the cells' viability was evaluated by the Alamar blue colorimetric assay (alamarBlue, Thermo Fisher) following manufacturer's instruction. Briefly, 100 μL of the ready-to-use Alamar solution was added to each well containing cell-seeded specimens and the plate was incubated 4 h at 37 °C in the dark. Then, an aliquot of 100 μl of each supernatant was collected and transferred to a new black-bottom 96-well plate; after gently shaking the plate, fluorescence intensity was detected at 600 nm with a spectrophotometer (Victor, IBM). Mirror-polished specimens were considered as control.

Statistical Analysis of Data: Biological experiments were performed using three replicates/specimen for each assay. Results were statistically analyzed using the SPSS software (v.20.0, IBM, USA). Control and test groups were compared by the one-way ANOVA using the Tukey's test as posthoc analysis. Significant differences were established at $p < 0.05$.

Conflict of Interest

The authors declare no conflict of interest.

Data Availability Statement

The data that support the findings of this study are available from the corresponding author upon reasonable request.

[1] J. Prathapachandran, N. Suresh, *Dent. Res. J.* **2012**, *9*, 516.

[2] C. Marambio-Jones, E. M. V. Hoek, *J. Nanoparticle Res.* **2010**, *12*, 1531.

[3] S. Ferraris, S. Spriano, *Mater. Sci. Eng., C* **2016**, *61*, 965.

[4] L. Kvitek, A. Panacek, R. Prucek, J. Soukupova, M. Vanickova, M. Kolar, R. Zboril, *J. Phys. Conf. Ser.* **2011**, *304*, 012029.

[5] J. P. Ruparelia, A. Kumar, S. P. Duttagupta, *Acta Biomater.* **2008**, *4*, 707.

[6] M. A. Raza, Z. Kanwal, A. Rauf, A. N. Sabri, S. Riaz, S. Naseem, *Nanomaterials* **2016**, *6*, 74.

[7] T. C. Dakal, A. Kumar, R. S. Majumdar, V. Yadav, *Front. Microbiol.* **2016**, *7*, 1.

[8] M. Rai, K. Kon, A. Ingle, N. Duran, S. Galdiero, M. Galdiero, *Appl. Microbiol. Biotechnol.* **2014**, *98*, 1951.

[9] S. Ferraris, S. Spriano, M. Miola, E. Bertone, V. Allizond, A. M. Cuffini, G. Banche, *Surf. Coat. Technol.* **2018**, *344*, 177.

[10] S. Ferraris, A. Venturello, M. Miola, A. Cochis, L. Rimondini, S. Spriano, *Appl. Surf. Sci.* **2014**, *311*, 279.

[11] S. Ferraris, A. Vitale, E. Bertone, S. Guastella, C. Cassinelli, J. Pan, S. Spriano, *Mater. Sci. Eng., C* **2016**, *60*, 384.

[12] S. Ferraris, S. Spriano, G. Pan, A. Venturello, C. L. Bianchi, R. Chiesa, M. G. Faga, G. Maina, E. Vernè, *J. Mater. Sci. Mater. Med.* **2011**, *22*, 533.

[13] S. Ferraris, S. Yamaguchi, N. Barbani, M. Cazzola, C. Cristallini, M. Miola, E. Vernè, S. Spriano, *Acta Biomater.* **2020**, *102*, 468.

[14] S. Ferraris, A. Cochis, M. Cazzola, M. Tortello, A. Scalia, S. Spriano, L. Rimondini, *Front. Bioeng. Biotechnol.* **2019**, *7*, 1.

[15] S. Spriano, S. Ferraris, G. Pan, C. Cassinelli, E. Vernè, *J. Mech. Med. Biol.* **2015**, *15*, 1540001.

[16] M. Metikoš-Huković, A. Kwokal, J. Piljac, *Biomaterials* **2003**, *24*, 3765.

[17] M. Textor, C. Sittig, V. Frauchiger, S. Tosatti, D. Brunette, in *Titanium in Medicine* (Eds: D. M. Brunette, P. Tengvall, M. Textor, P. Thomsen), Springer-Verlag, Berlin, Heidelberg **2001**, pp. 172–230.

[18] L. Burgos-Asperilla, M. C. García-Alonso, M. L. Escudero, C. Alonso, *Acta Biomater.* **2010**, *6*, 652.

[19] M. C. Biesinger, L. W. M. Lau, A. R. Gerson, R. S. C. Smart, *Appl. Surf. Sci.* **2010**, *257*, 887.

[20] A. Shchukarev, B. Ö. Malekzadeh, M. Ransjö, P. Tengvall, A. Westerlund, *J. Electron Spectrosc. Relat. Phenom.* **2017**, *216*, 33.

[21] X. Zhang, S. Ferraris, E. Prenesti, E. Verné, *Appl. Surf. Sci.* **2013**, *287*, 329.

[22] P. Dong, J. Feng, D. Zhang, C. Li, Q. Shan Shi, X. Xie, *React. Funct. Polym.* **2020**, *153*, 104609.

[23] D. Musino, C. Rivard, G. Landrot, B. Novales, T. Rabilloud, I. Capron, *J. Colloid Interface Sci.* **2021**, *584*, 360.

[24] G. Riccucci, M. Cazzola, S. Ferraris, V. A. Gobbo, M. Guaita, S. Spriano, *Mater. Des.* **2021**, *206*, 109776.

[25] J. Sánchez-Bodón, J. A. Del Olmo, J. M. Alonso, I. Moreno-Benítez, J. L. Vilas-Vilela, L. Pérez-Álvarez, *Polymers* **2022**, *14*, 165.

[26] L. Zhao, H. Wang, K. Huo, L. Cui, W. Zhang, H. Ni, Y. Zhang, Z. Wu, P. K. Chu, *Biomaterials* **2011**, *32*, 5706.

[27] B. Yu, K. M. Leung, Q. Guo, W. M. Lau, J. Yang, *Nanotechnology* **2011**, *22*, 115603.

[28] E. Albiter, M. A. Valenzuela, S. Alfaro, G. Valverde-aguilar, *J. Saudi Chem. Soc.* **2015**, *19*, 563.

[29] L. Zhao, H. Wang, K. Huo, L. Cui, W. Zhang, H. Ni, Y. Zhang, Z. Wu, P. K. Chu, *Biomaterials* **2011**, *32*, 5706.

[30] G. Ren, D. Hu, E. W. C. Cheng, M. A. Vargas-reus, P. Reip, R. P. Allaker, *Int. J. Antimicrob. Agents* **2009**, *33*, 587.

[31] A. Shivaram, S. Bose, A. Bandyopadhyay, *Acta Biomater.* **2017**, *58*, 550.

[32] G. Liu, Y. Li, M. Yan, J. Feng, J. Cao, M. Lei, Q. Liu, X. Hu, W. Wang, X. Li, *J. Mater. Sci. Technol.* **2022**, *116*, 180.

[33] G. Balato, V. de Matteo, T. Ascione, R. de Giovanni, E. Marano, M. Rizzo, M. Mariconda, *BMC Musculoskelet. Disord.* **2021**, *22*, 1006.

[34] T. Bruna, F. Maldonado-Bravo, P. Jara, N. Caro, *Int. J. Mol. Sci.* **2021**, *22*, 7202.

[35] E. M. Sussman, B. J. Casey, D. Dutta, B. J. Dair, *J. Appl. Toxicol.* **2015**, *35*, 631.

[36] R. D. Holbrook, K. Rykaczewski, M. E. Staymates, *J. Mater. Sci. Mater. Med.* **2014**, *25*, 2481.

[37] M. Akter, M. T. Sikder, M. M. Rahman, A. K. M. A. Ullah, K. F. B. Hossain, S. Banik, T. Hosokawa, T. Saito, M. Kurasaki, *J. Adv. Res.* **2018**, *9*, 1.

[38] S. Spriano, E. Verné, S. Ferraris, EP2739323A1, **2011**.

[39] P. Schlossmacher, D. O. Klenov, B. Freitag, S. Von Harrach, A. Steinbach, *Microsc. Anal. Nanotechnol. Suppl.* **2010**, *24*, S5.

[40] L. R. Rivera, A. Cochis, S. Biser, E. Canciani, S. Ferraris, L. Rimondini, A. R. Boccaccini, *Bioact. Mater.* **2021**, *6*, 1479.

[41] A. Cochis, B. Azzimonti, C. Della Valle, E. De Giglio, N. Bloise, L. Visai, S. Cometa, L. Rimondini, R. Chiesa, *Biomaterials* **2016**, *80*, 80.